

Study of the Impact Response of Glass Fiber Reinforced Aluminium Laminates for Conical and Blunt Nose Projectiles

Tanzeem ul Hasan¹, Raisuddin Ansari²

^{1,2}Department of Mechanical Engg., ZHCET, Aligarh Muslim University, Aligarh, India

ABSTRACT

It is known that fiber metal laminates (FML) as one of hybrid materials with thin metal sheets and fiber/epoxy layers have the characteristics of the excellent damage tolerance, fatigue and impact properties with a relatively low density. Therefore, the mechanical components using FML can contribute the enhanced safety level of the sound construction toward the whole body. In the present study, the impact performance of glass fibers reinforced aluminum laminates (GFRAL) is investigated by experiments and numerical simulations. Impact tests are carried out with the blunt and conical nose projectiles of mass 29 g within sub ordnance velocity range (50-150 m/s). Two different thicknesses viz. 2.6 mm and 3.1 mm are impacted. Dynamic non-linear transient analyses are also accomplished using finite element analysis software, ABAQUS.

Results show higher ballistic limit for conical nose projectile compared to blunt nose. Also, failure mode in case of conical nose projectile impact is petalling with localized delamination of the GFRAL specimen. In case of blunt nose projectile impact plugs are sheared off from front (aluminium) plate and middle (GFRP) plate. One thing is common in failure modes by both conical and blunt nose projectiles, *delamination of GFRP plate in itself*.

Keywords - Impact Performance, Fiber Metal Laminates (FML), Glass Fiber Reinforced Aluminium Laminates (GFRAL), Sub Ordnance Range, Numerical Simulation.

I. Introduction

Weight reduction and improved damage tolerance characteristics were the prime drivers to develop new family of materials for the aerospace/aeronautical industry. For this objective, new lightweight fiber metal laminates (FML) has been developed. The combination of metal and polymer composite laminates can create a synergistic effect on many properties. The mechanical properties of FML show improvements over the properties of both metal alloys and composite materials individually. Strength of FML depends upon type of fiber (viz. carbon fiber, glass fiber etc.), the used metal and various other factors viz. fiber architecture, weaving quality and the resin.

High stiffness of fibers allows for good efficient crack bridging and therefore very low crack growth rates. At the same time, the presence of a metal layer is very favorable for the impact properties. The combination of high stiffness and strength with good impact property gives FML a great advantage for space applications.

Recent advances using composite in modern aircraft constructions were reviewed and carbon fibers were particularly argued in terms of design, manufacturing by Soutis [1]. He summarized that because of significant weight savings, carbon fiber reinforced composites are to be utilized for future aircraft construction. For secondary structures, weight reduction up to 40% is feasible by using composites instead of light weight metal alloys, while for primary structures, such as wings and fuselages, 20% or more is realistic. Advancement in fabric engineering and emergence of new type of reinforcement has resulted in new form of composite materials with higher performance characteristics. Utilization of these reinforcement solely or in combination for impact application requires detail understanding of their response towards impact loading. A significant amount of work [2-4] has already been published on polymer composite structures under high velocity impact, different aspects have been reviewed Cuniff [5] observed that loosely woven fabrics and fabrics with unbalanced weaves result in inferior ballistic performance. Kim and Sham [6] showed that cross woven fabric composites exhibits higher fracture toughness as compared to unidirectional laminates under high velocity impact. P. Soltani, M. Keikhosravy *et. al.* investigated the tensile behaviour of glass fiber reinforced aluminium laminates (GLARE) [7]. *They recommended use of composite laminates with fibers aligned to load directions.* Alireza *et. al.* [8] investigated the effect of reinforcement type on high velocity impact response of GFRP in velocity range of 80-160 m/s. Five different types of reinforcements are investigated viz. chopped strand mat (CSM), plain weave, satin weave, unidirectional and cross ply unidirectional. For the specimens of thickness 3 mm, highest ballistic limit was found for cross ply (95 m/s) UD layup followed by UD and satin weave (86.4 m/s). In case of 6 mm thickness specimens, highest ballistic limit was found for plain weave type (146 m/s) followed by CSM (140 m/s). S.H. Song *et. al.* [9] carried out drop impact test and numerical

modeling on CARAL (carbon fiber reinforced aluminium laminates). Two layers of CFRP (thickness 0.2 mm each) were laminated in between three layers of aluminium of thickness 0.5 mm each. Impact energy levels 2.35 J and 9.40 J. The specimen showed no critical damage area at 2.35 J, but in case of 9.40 J it shows fiber and matrix cracking in CFRP layers. In the present study, the impact performance of glass fibers reinforced aluminum laminates (GFRAL) is investigated by experiments and numerical simulations. Impact tests are carried out with the blunt and conical nose projectiles of mass 29 g within sub ordnance velocity range (50-150 m/s). Two different thicknesses of 255 mm circular plates viz. 2.6 mm and 3.1 mm are impacted. Dynamic non-linear transient analyses are also accomplished using finite element analysis software, ABAQUS. The experiment results and numerical results are compared.

II. Experimental Analysis

Impact tests are carried out on pneumatic impactor shown in Fig. 3, embedded with velocity measuring devices e.g. velocity sensors, oscilloscope and DC supply etc.

Material and Projectiles

GFRAL specimens were made by laminating cross woven (0° and 90°) E glass/epoxy (GFRP) with pure commercial aluminum Fig. 1. Adhesive films of ARALDITE were inserted in between the interfaces of GFRP and aluminum sheets to laminate them. Before laminating the sheets, interfaces are washed with acetone in order to remove any oil film to ensure flawless bonding. After laminating, the sheets are cured under constant pressure for about 30 hours at room temperature.

The GFRAL is made in two thicknesses viz. 2.6 mm and 3.1 mm, by laminating two different thicknesses of GFRP viz. 1 mm and 1.5 mm and keeping thickness of the front and rear aluminium plates 0.8 mm. The diameter of the GFRAL equals 255 mm having eight holes of 8 mm diameter arranged on a 230 mm pitch circle diameter in order to clamp the target by means of two circular holding rings.

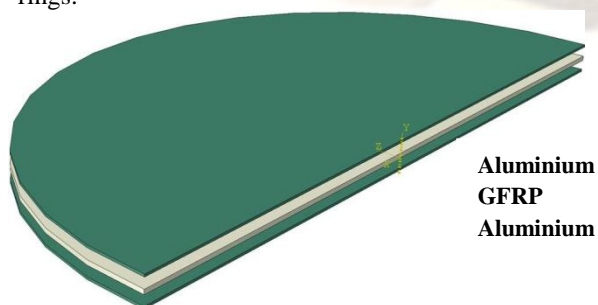


Fig. 1 The GFRAL Layup



Fig. 2 The Blunt and Conical Nose Projectiles Used in the Study.

Two solid projectiles of different nose shapes i.e. conical (45° nose angle) and blunt nose, both having a mass of 29 g and 12.8 mm diameter, are used in the present study (Fig. 3). The projectiles are made of EN-24 steel, manufactured on a lathe machine. Impact tests are carried out by varying the impact velocity.

III. Numerical Simulation Using ABAQUS

3.1 Damage Initiation Criteria for Aluminium

To simulate the impact test, a damage model is essential to predict the onset of damage in aluminium and GFRP plates. To predict damage in aluminium an elasto-viscoplastic material model presented by Johnson and Cook was employed [10, 16]. The Johnson and Cook model is the product of three material characteristics namely, strain hardening, strain rate hardening and temperature softening and is expressed as:

$$\sigma_{yield} = [A + B(\bar{\epsilon}^p)^n][1 + C \ln(\dot{\epsilon}^*)][1 + (T^*)^m] \quad (1)$$

Where A, B, n, C, m are material parameters measured at or below the transition temperature, $\bar{\epsilon}^p$ is the equivalent plastic strain, $\dot{\epsilon}^*$ is the ratio of equivalent plastic strain rate and reference strain rate, T^* is the non-dimensional temperature defined below as:

$$T^* = \frac{T - T_{room}}{T_{melt} - T_{room}} \quad (2)$$

Where T is the current temperature, T_{melt} is the melting temperature and $T_{transition}$ is the transition temperature defined as the one at or below which there is no temperature dependence on the expression of the yield stress. The material parameters must be measured at or below the transition temperature. When $T > T_{melt}$, the material will be melted and will behave like a fluid; there will be no shear resistance since $\sigma_o = 0$:

$$\sigma_{yield} = [A + B(\bar{\epsilon}^p)^n][1 + (T^*)^m] \quad (3)$$

Where σ_o is the static yield stress. In the modelling these parameters are used from the literature [11].

Johnson and Cook Dynamic Failure Criteria

The Johnson and Cook dynamic failure model is based on the value of equivalent plastic

strain at element integration points; failure is assumed to occur when the damage parameter exceeds 1. The damage parameter, D, is defined as:

$$D = \sum \frac{\Delta \varepsilon^{pl}}{\varepsilon_f^{pl}} \quad (4)$$

Where $\Delta \varepsilon^{pl}$ an increment of the equivalent plastic strain is, ε_f^{pl} is the strain at failure and the summation is performed over all increments of the analysis. The strain at failure ε_f^{pl} is assumed to be dependent on a non-dimensional plastic strain rate, $\dot{\varepsilon}^*$; a dimensionless pressure deviatoric stress ratio or the stress triaxiality ratio, σ^* and the non-dimensional temperature, T^* as:

$$\varepsilon_f^{pl} = [D_1 + D_2 e^{(D_3 \sigma^*)}] [1 + D_4 \ln(\dot{\varepsilon}^*)] [1 + D_5 T^*] \quad (5)$$

Where D1-D5 are failure parameters measured at or below the transition temperature and $\dot{\varepsilon}^*$ is the reference strain rate. The first set of brackets in the Johnson and Cook damage criteria is intended to represent the observation that the strain to fracture decreases as hydrostatic tension increases. The second bracket represents the effect of strain rate on material ductility, while the third bracket gives the effect of thermal softening on material ductility. The values of above parameters have been taken from [11].

3.2 Damage Initiation Criteria for GFRP

To simulate the damage in GFRP an elastic-brittle materials with anisotropic behavior is employed. The implemented model uses the *Hashin damage initiation criteria* [12]. This criteria consider four different damage initiation mechanisms: fiber tension, fiber compression, matrix tension and matrix compression. The initiation criteria have the following general forms:

Fiber tension ($\hat{\sigma}_{11} \geq 0$):

$$F_f^t = \left(\frac{\hat{\sigma}_{11}}{X^T} \right)^2 + \alpha \left(\frac{\hat{\tau}_{12}}{S^L} \right)^2$$

Fiber compression ($\hat{\sigma}_{11} < 0$):

$$F_m^c = \left(\frac{\hat{\sigma}_{11}}{X^C} \right)^2$$

Matrix tension ($\hat{\sigma}_{22} \geq 0$):

$$F_m^t = \left(\frac{\hat{\sigma}_{22}}{Y^T} \right)^2 + \left(\frac{\hat{\tau}_{12}}{S^L} \right)^2$$

Matrix compression ($\hat{\sigma}_{22} < 0$):

$$F_m^c = \left(\frac{\hat{\sigma}_{22}}{2S^T} \right)^2 + \left[\left(\frac{Y^C}{2S^T} \right)^2 - 1 \right] \frac{\hat{\sigma}_{22}}{Y^C} + \left(\frac{\hat{\tau}_{12}}{S^L} \right)^2 \quad (6)$$

Where X^T is the longitudinal tensile strength, X^C is the longitudinal compressive strength, Y^T is the transverse tensile strength, Y^C is the transverse compressive strength, S^L is the longitudinal shear strength, S^T is the transverse shear strength, and α is a coefficient that determines the contribution of the shear stress to the fiber tensile initiation criterion, respectively. And

$\hat{\sigma}_{11}$, $\hat{\sigma}_{22}$, $\hat{\tau}_{12}$ are components of the effective stress tensor, $\hat{\sigma}$. These values are used from the literature [13].

3.3 Finite Element Analysis

A 2D- axisymmetric model is created (due to symmetry) with ABAQUS/ Explicit. The target Plate (GFRAL) is modelled as deformable part. The projectiles are modelled as analytical rigid parts and no property is assigned except the mass and initial velocity to the *reference point*. Cohesive interaction is given in between the interfaces of middle GFRP plate and upper and lower aluminium plates. Surface to surface contact is given between the projectile and the plate. *Penalty contact algorithm* was employed in the mechanical constraint formulation with projectile as the master surface and plate as node based slave surface with coefficient of friction 0.05.

IV. Results and Discussion

4.1 Failure Mode and Deformation of the Plate

In case of conical nose projectile GFRAL fails are petalling accompanied with local delamination of the member plates viz. aluminium-gfrp-aluminium plates – as shown in Fig. 4 (a). The GFRAL specimen is delaminated in nearby region of impact zone. *The GFRP gets delaminated in itself* along the fault interfaces introduced during manufacturing [15].

In case of blunt nose projectile plugging are dominant mode of failure in case of blunt nose projectile. A clear cut plug is sheared off from the front aluminium plate and GFRP plate. The plug of the GFRP gets splitted into layers. A plug get sheared off from the rear aluminium plate but remains attached to the plate as shown in Fig. 4 (b).

Figure 5 (a) and (b) shows the deformation of the plate for both the thicknesses. Deformation is more in 2.6 mm thick GFRAL for both the projectiles (about 20 mm) compared to 3.1 mm thickness (13 mm). Also there is no significant effect of nose shape on deformation. Also deformation area decreases little bit at higher impact velocity.

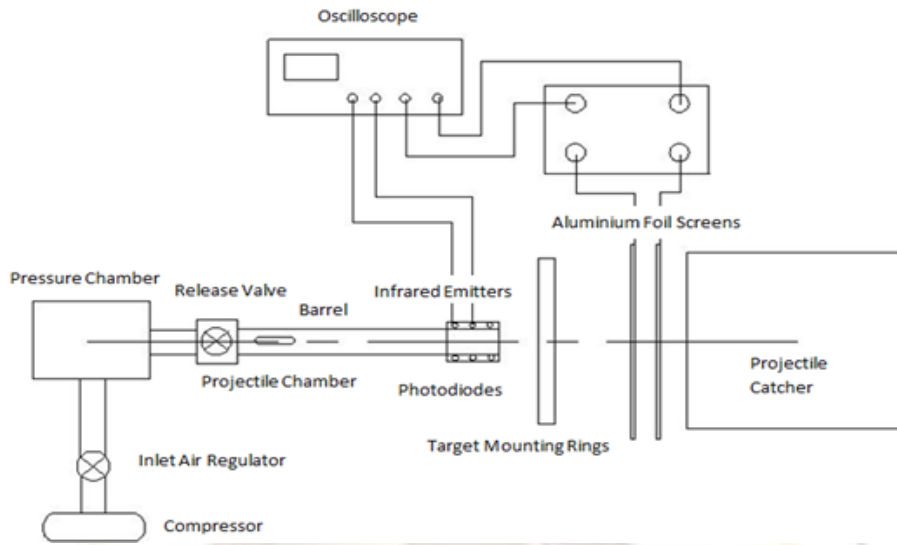


Fig. 3 Schematic Diagram of the Experimental Setup.



Fig. 4 Failure of GFRAL by (a) Conical and (b) Blunt Nose Projectiles.

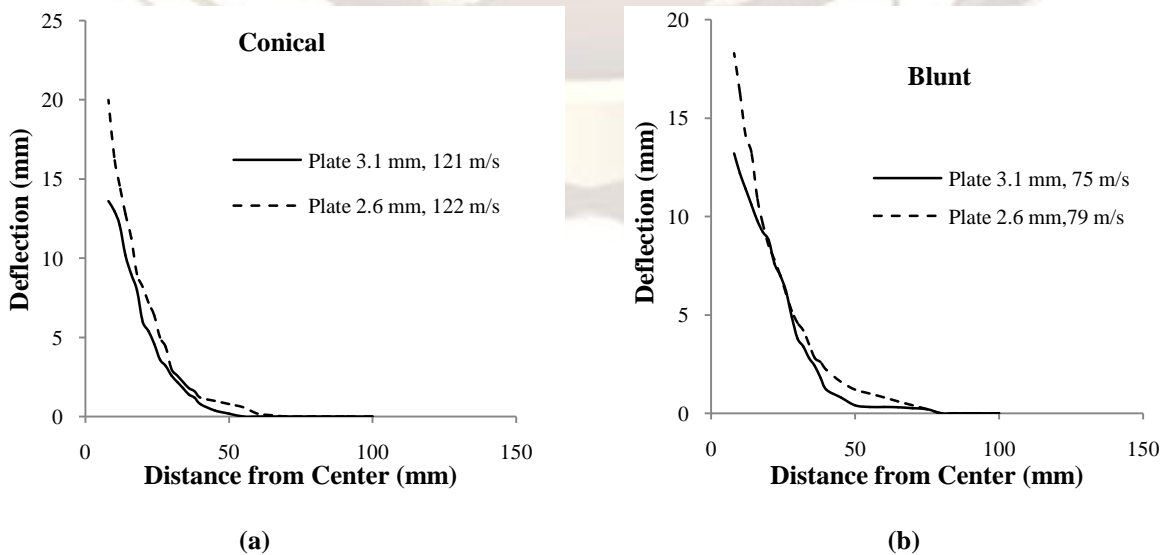


Fig. 5 Deformation of the Plate.

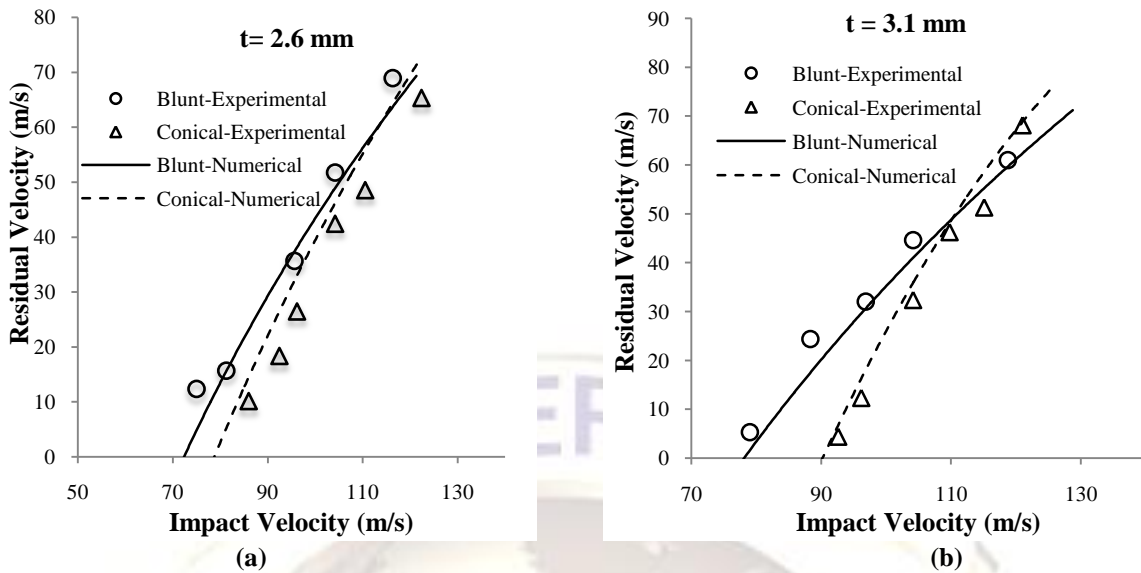


Fig. 6 Variation of Residual Velocity with Impact Velocity for both the Thicknesses.

4.2 Ballistics Performance of the GFRAL

Ballistic limit and effect of nose shape on residual velocity and energy absorbed is studied for the GFRAL. Figure 6 (a) and (b) shows the variation of residual velocity for both the thicknesses. Residual velocity is found more for

blunt nose projectile as compared to the conical nose projectile.

At higher impact velocity, residual velocity is more for conical nose projectile. Also increase in residual velocity is more rapid than the blunt nose projectile.

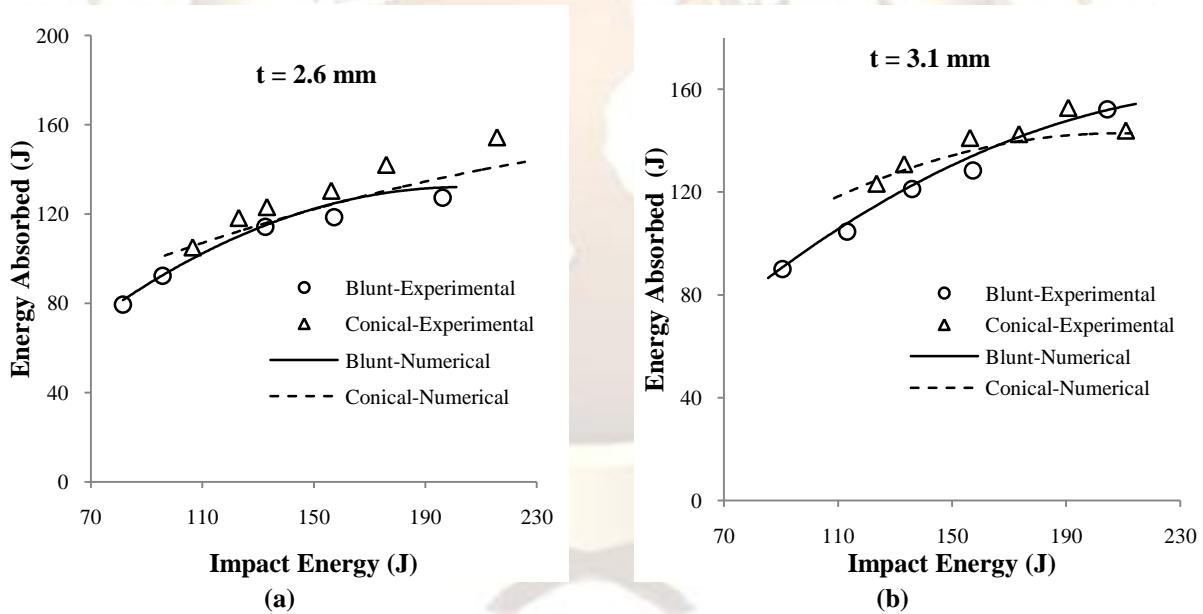


Fig. 7 Variation of Energy Absorbed with Impact Energy.

Figure 7 shows the energy absorption results of the specimen. In case of 2.6 mm thickness, energy absorption is higher for conical and this is more evident at low impact velocity. At higher impact velocity, this difference of energy absorption between conical and blunt nose projectiles decreases. In case of 3.1 mm thickness, energy absorption is higher for

conical nose projectile at lower impact velocity and drops down the blunt nose at higher impact velocity.

From the above results it has been observed during projectile-plate impacts that *the nose shape of the projectile used changes the energy absorbed, the failure mode and the ballistic limit*. Energy absorption is higher for conical nose projectile than blunt nose projectile at impact velocity smaller than

110 m/s. At impact velocity higher than 110 m/s, the energy absorption for conical nose projectile decreases rapidly. At these higher impact velocities, the energy absorbed for conical nose projectile is lower than that of the blunt nose.

Figure 8 shows the effect of target thickness on residual velocity. It can be observed for both the projectiles, residual velocity decreases as target thickness increases. For conical nose projectile (a), the difference between the residual velocities for both the thicknesses decreases as impact velocity increases. But in case of blunt nose projectile, this difference is almost constant (b).

Figure 9 shows the effect of target thickness on energy absorption for conical nose and blunt nose projectiles. The graphs depict energy absorption increases with increases in target thickness. For conical nose projectile (a) the difference in energy

absorption is higher at low impact velocities and reduces at higher impact velocities. But in case of blunt nose projectile this difference increases as impact velocity increases (b).

Ballistic Limit

Table 1 shows the experimental and numerical ballistic limits for different combinations. Ballistic limit is high for conical nose projectile as compared to the blunt nose projectile for both the thicknesses. It shows that conical nose projectile experiences more resistance in passing through GFRAL plate.

The ballistic limit increases as thickness of the target GFRAL increases for both the projectiles. Increases in ballistic limit with thickness for both the projectiles is almost at same rate i.e. there is no rapid increase in ballistic limit as thickness increases from 2.6 mm to 3.1 mm.

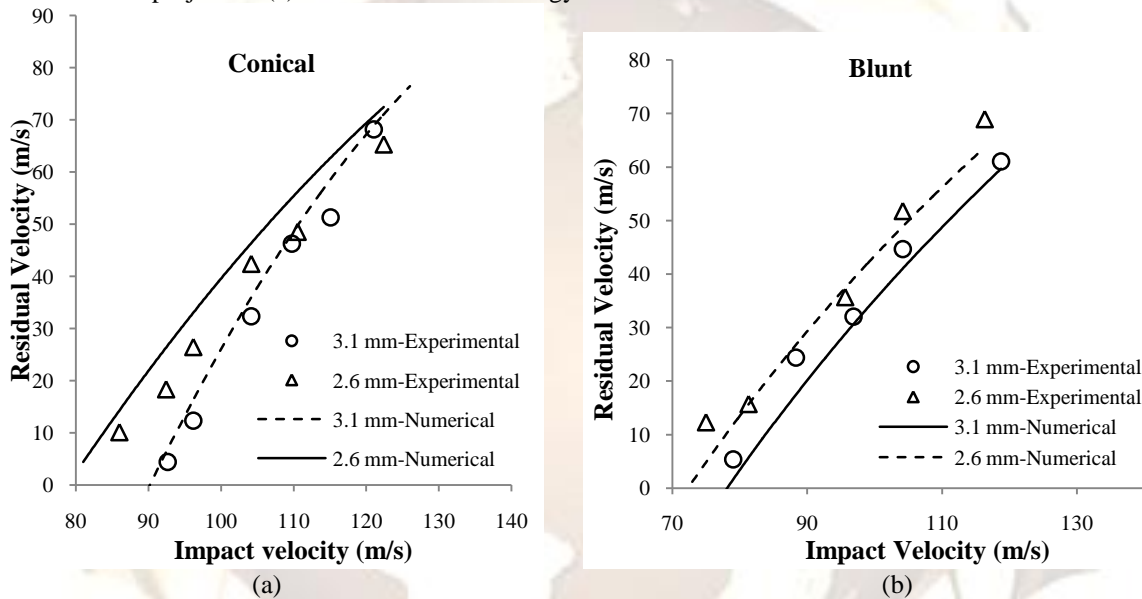


Fig. 8 Effect of Target Thickness on Residual Velocity.

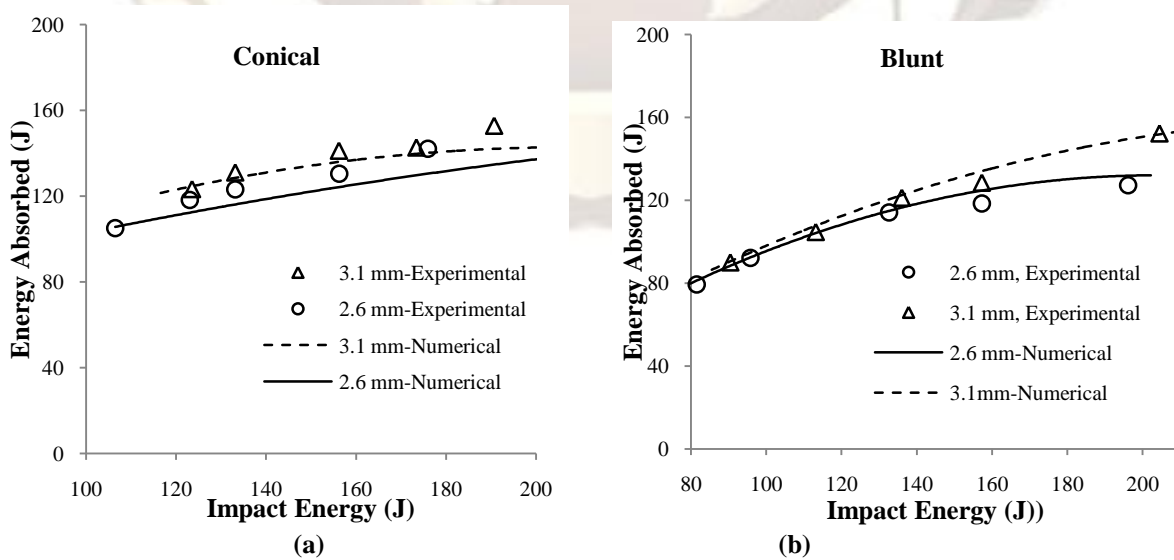


Fig. 9 Effect of Target Thickness on Energy Absorption.

Table 5.1 Ballistic Limit for Blunt and Conical Nose Projectiles.

S. No.	Plate Thickness (mm)	Ballistic Limit for Blunt Nose Projectile (m/s)		Ballistic Limit for Conical Nose Projectile (m/s)	
		Experimental	Numerical	Experimental	Numerical
1	2.6	67.7	68.5	79.72	78
2	3.1	74.8	76.7	89.8	88.9

V. Conclusion

(a) Failure mode of the composite plate GFRAL in case of conical nose projectile is petalling accompanied with localized delamination of the specimen.

Composite plate gets delaminated in nearby region of the impact zone. This delamination zone slightly decreases as impact velocity increases. The GFRP of the composite plate get delaminated in itself. The GFRP get splitted, usually, into three (3) pieces along the thickness. This is due to faults induced in the matrix (resin) during manufacturing. These faults get delaminated due to vibrations generated by striking of the projectile. Number of petals is equal in middle GFRP plate and successive rear aluminium plate.

(b) Failure mode of composite plate in case of blunt nose projectile is shearing of the plate. A clear cut plug is obtained from the front aluminium plate and middle GFRP plate. The plug obtained from the GFRP plate was splitted into three pieces along the thickness. Failure of the rear aluminium plate is somewhat combination of petalling and shearing. The plug formed but did not get separated from the plate and in half the region, petals formation occurs.

(c) Ballistic limit for both the thickness is found more for conical nose projectile (89.8 m/s and 79.2 m/s) as compared to the blunt nose projectile (74.75 m/s and 67.65 m/s) (Fig.7). Blunt nose projectile is found to be the better penetrator as compared to conical nose projectile i.e. blunt nose projectile requires less impact energy to penetrate the target.

So, the composite plate (GFRAL) exhibits more resistance to the conical nose projectile as compared to the blunt nose projectile.

(d) The deformation of plate 2.6 mm thickness is more (about 20 mm) as compared to 3.1 mm thickness (about 13 mm) for both the projectiles.

References

Journal Papers:

[1] C. Soutis, Fiber reinforced composites in aircraft constructions. *Prog Aerosp Sci*, 41, 2005, 141- 151.

[2] S. Abrate, Impact on laminated composites, recent advances in materials, *Appl Mech Rev*, 47(11),1994, 517-543.

[3] XL. Gao, JQ. Zheng, NV. David, Ballistic resistance body armour : contemporary and prospective materials and related protection mechanism. *Apple Mech Rev*, 2009, 62.05802 – 1- 05082-20.

[4] BA. Cheesman, TA Bogetti, Ballistic impact into fabric and compliant composite laminates, *Compos Struct*, 61, 2003, 16 –73.

[5] PM Cuniff, An analysis of the system effects in woven fabrics under ballistic impact. *Text Res J*, 69 (9), 1992, 495-509.

[6] JK. Kim, ML. Sham, Impact and delamination failure of woven fabric composites., *Compos Sci Technol*, 60 (5), 2000, 745-61.

[7] P. Soltani, M. Kiekhoosravy, RH Oskouei, C Soutis, Studying the tensile behaviour of GLARE laminates – A finite element approach. *Appl Compos Mater*, 18, 2011, 271-282.

[8] S. Alireza, F. Nargis, MH. Baheshty, Effect of reinforcement type on high velocity impact response of GRP plates using a sharp tip projectile. *Int J Impact Eng*, 38, 2011, 715-722.

[9] SH. Song, YS. Byun, TW. Ku, Experimental and numerical investigation on impact performance of carbon fiber reinforced aluminium laminate (CARAL), *JMST*, 26 (4), 2010, 327-332.

[10] Johnson GR, Cook WH. Fracture characteristics of three metals subjected to various strain, strain rates, temperatures and pressures. *Eng Fract Mech*, 21, 1985, 31-48.

[11] NK. Gupta, MA. Iqbal, GA. Sekhon, Experimental and numerical studies on the

behavior of thin aluminum plates subjected to impact by blunt and hemispherical nose projectiles. *Int J Imp Eng*, 32, 2006, 1921-1944.

- [12] Z. Hashin, A. Rotem, Fatigue criterion for fiber-reinforced materials. *Compos Mater*, 7, 1973, 448-64.
- [13] C. Menna, D. Aspron, G. Caprino, G. Lopresto, A. Prota, Numerical simulation of impact tests on GFRP composite laminates. *Int J Impact Eng*, 38, 2011, 677-685.

Books:

- [14] ABAQUS Analysis User's Manual, 2010. Version 6.10.

Theses:

- [15] KP. Subrat, U. Paritosh, *Failure characterization of FRP failure by scanning electron microscope technique*. B. Tech. Thesis, Department of Metallurgical and Materials Engineering, National Institute of Technology, Rourkela. India. 2008.

Proceedings Papers:

- [16] GR. Johnson, WH. Cook, A constitutive model and data for metals subjected to large strains, high strain rates and high temperatures. In: *Proceedings of the seventh international symposium on ballistics*, The Hague. 1983

